MULTISPECTRAL DATA FOR MAPPING SOIL TEXTURE: POSSIBILITIES AND LIMITATIONS

E. M. Barnes, M. G. Baker

ABSTRACT. *Soil maps derived from random or grid-based sampling schemes are often an important part of precision crop management. Sampling and soil analysis to derive such maps require a large investment of both time and money. Aerial photos have been used as a soil mapping aid for years. Studies have shown such an approach can be useful for defining management units in precision farming, but these studies are often limited to a single field, not an entire farming operation. In this study, multispectral airborne [green, red, near infrared (NIR), and thermal] and satellite (SPOT and Landsat TM) data were used to derive soil textural class maps for 350 ha of a 770 ha research and demonstration farm in Maricopa, Arizona. These maps were compared to soil textural analysis results from samples in the top 30 cm of the soil profile at an approximate grid spacing of 120 m. Differences in tillage, residue, soil moisture, etc. between fields limited the accuracy of spectral classification procedures when applied across the entire study area. However, using spectral classification procedures on a field-by-field basis, it was possible to map areas of soil textural class with reasonable accuracy. These results are specific to the study area and may not apply at other locations due to the numerous factors that can contribute to a soil's spectral response. Classification procedures were also used with vegetation present over the study area later in the season. Resulting vegetation classes may be helpful in deciding if soil classes impact crop development enough to warrant different management practices.*

Keywords. *Remote sensing, Precision farming, Soil mapping.*

Site-specific or precision crop management had its earliest beginnings in efforts to account for within-field soil type variations. First applications for mapping differences in soil properties relied on grid-based sampling and statistical interpolation between points (Nielsen et al., 1995). While this technique is still used, the expense of collecting and analyzing the number of samples can be significant and in some cases economically prohibitive (Ferguson et al., 1996). Alternatives to direct soil sampling that have been investigated include analysis of previous year's yield maps (Cambardella et al., 1996), electromagnetic induction (Jaynes, 1996), examination of topographic information (Bell et al., 1995), and use of remotely sensed imagery (Thompson and Robert, 1995). The use of remotely sensed data has met with varying degrees of success for mapping different soil properties. Strong correlation between soil properties such as organic matter content or textural distribution and spectral data have been found in a laboratory setting (Dalal and Henry, 1986) or for a single field (Milfred and Kiefer, 1976). However, few studies have examined the application of these techniques to an entire farm. The objective of this study was to generate maps of soil texture over 565 ha of a research farm in Maricopa, Arizona, from multispectral images acquired by aircraft and satellite platforms. These image-based maps were compared to a soil map generated by kriging procedures. Factors limiting the utilization of remotely sensed technology for soil mapping were also evaluated.

Article was submitted for publication in November 1999; reviewed and approved for publication by the Information & Electrical Technologies Division of ASAE in June 2000. Presented as ASAE Paper No. 99-1138.

Mention of a trade name, proprietary product, or specific equipment does not constitute a guarantee or warranty by the authors or the USDA and does not imply approval of a product to the exclusion of others which may be suitable.

The authors are **Edward M. Barnes**, ***ASAE Member Engineer***, Agricultural Engineer, and **Michael G. Baker**, Research Specialist, USDA-Agricultural Research Service, U.S. Water Conservation Laboratory, Phoenix, Arizona. **Corresponding author:** Edward M. Barnes, U.S. Water Conservation Laboratory, 4331 E. Broadway Rd., Phoenix, AZ 85040, phone: 602.379.4356, fax 602.379.4355, e-mail: <ebarnes@uswcl.ars.ag.gov>.

PREVIOUS STUDIES

Aerial imagery has been used to aid in soil mapping for over 60 years (Bushnell, 1932), and with advances in digital imaging, such information can now be directly input to a geographical information system (GIS). In laboratory studies, NIR reflectance has successfully quantified soil properties such as moisture, organic carbon, and total nitrogen (Dalal and Henry, 1986; Shonk et al., 1991). Similar relationships have also been found at the field level. For example, Milfred and Kiefer (1976) found soil patterns over a 12 ha field were most obvious three days after a rainfall in color photographs. Color infrared film was also used in the study, but no significant difference was found between the two methods in the ability to distinguish soil patterns. The same spatial patterns were also seen in a corn crop that was later planted in the field. The patterns were attributed to topography (as it affected the distribution of rainfall infiltration), and variations in thickness of silty material over a sand and gravel substratum. Thompson and Robert (1995) found aerial imagery allowed for fewer soil samples than interpolation techniques such as kriging or distance-weighted interpolation. Pocknee et al. (1996) provide an example where an aerial photograph of a bare

field was used to map soil properties by a "directed soil sampling" method. The method worked well for mapping soil phosphorus, but performed poorly for soil pH. Estimation of soil particle size has been proposed using a combination of visible, NIR, and thermal infrared data (Salisbury and D'Aria, 1992).

Aerial imagery has also been a useful tool to designate management zones by examining spatial patterns of a vegetation index, which can be correlated with variations in crop biomass (Yang and Anderson, 1996). Yang and Anderson (1996) utilized green, red, and NIR images of vegetated fields to classify areas of a field to be managed differently with respect to the agricultural inputs they received. This was accomplished by first performing unsupervised classification on multispectral data and then taking soil and plant samples in the resulting classes to determine the proper management approaches for each class. Airborne data have also found applications in mapping soil salinity (Wiegand et al., 1994; Verma et al., 1994), and plant nitrogen status (Bausch et al., 1996; Blackmer and White, 1996). An overview of the application of remotely sensed data to other precision crop management practices is provided by Moran et al. (1997b).

Materials and Methods

This research was conducted at the University of Arizona's Maricopa Agricultural Center (MAC). MAC is a 770 ha research and demonstration farm located approximately 37 km south of Phoenix, Arizona. The analysis was limited to the 565 ha demonstration portion of the farm as fields are larger and farming practices were more consistent than on the research portion. Additionally, crops were present in some fields during the time imagery was available. Therefore, the image-based analysis was further limited to 350 ha where the fields were fallow or recently tilled. This 350 ha area is represented by the fields with identification numbers in figure 1a. All of the soil sampling locations were used in the kriging procedures.

Soil Samples

Soil data used in this study were collected by Post et al. (1988) from May 1984 until January 1987. Characteristics of the three primary NRCS soil map units (USDA-SCS, 1991) that cover the farm are listed in table 1, with their spatial extent illustrated on figure 1a. Five hundred fifty-five Ap surface horizon (0 to 30 cm depth) soil samples were collected on a grid design system across the demonstration portion of the farm (typical grid spacing was 120 m). The sampling locations are shown on figure 1a. Of the 555 samples, 303 were in the fields used to evaluate the image-based procedures. For each of these samples, textural fractions of sand, silt and clay were determined and the location recorded in a UTM coordinate system. Sampling locations were determined to the nearest meter based on relative distance from field boundaries which

Table 1. Properties of the three soil map units in the study area from Post et al. (1988)

Soil Series*	Textural Class†	Depth (cm)	Sand (%)	Clay (%)	Bulk Density (g cm^{-3})	Organic Matter (%)	CEC (meq/ 100 g)
MO	SL	0-30	65-75	10-15	1.4-1.6	0.4-0.6	8-10
MO	SL	30-100	65-75	10-15	1.4-1.6	0.1-0.2	7-9
CG	SCL	0-30	45-55	22-27	1.45-1.55	0.8-1.2	13-16
CG	SCL	30-100	45-55	22-27	1.45-1.55	0.2-0.4	12-15
TR	CL	0-30	25-45	27-40	1.40-1.55	1.2-1.5	24-27
TR	SCL	30-100	45-55	22-27	1.40-1.55	0.6-0.8	15-18

* MO is Mohall (fine-loamy, mixed, hyperthermic *Typic Haplargid*); CG is Casa Grande (fine-loamy, mixed, hyperthermic *Typic Natrargids*); TR is Trix (fine-loamy, mixed, hyperthermic *Typic Torrifluvents*).

† SL is sandy loam, SCL is sandy clay loam, and CL is clay loam.

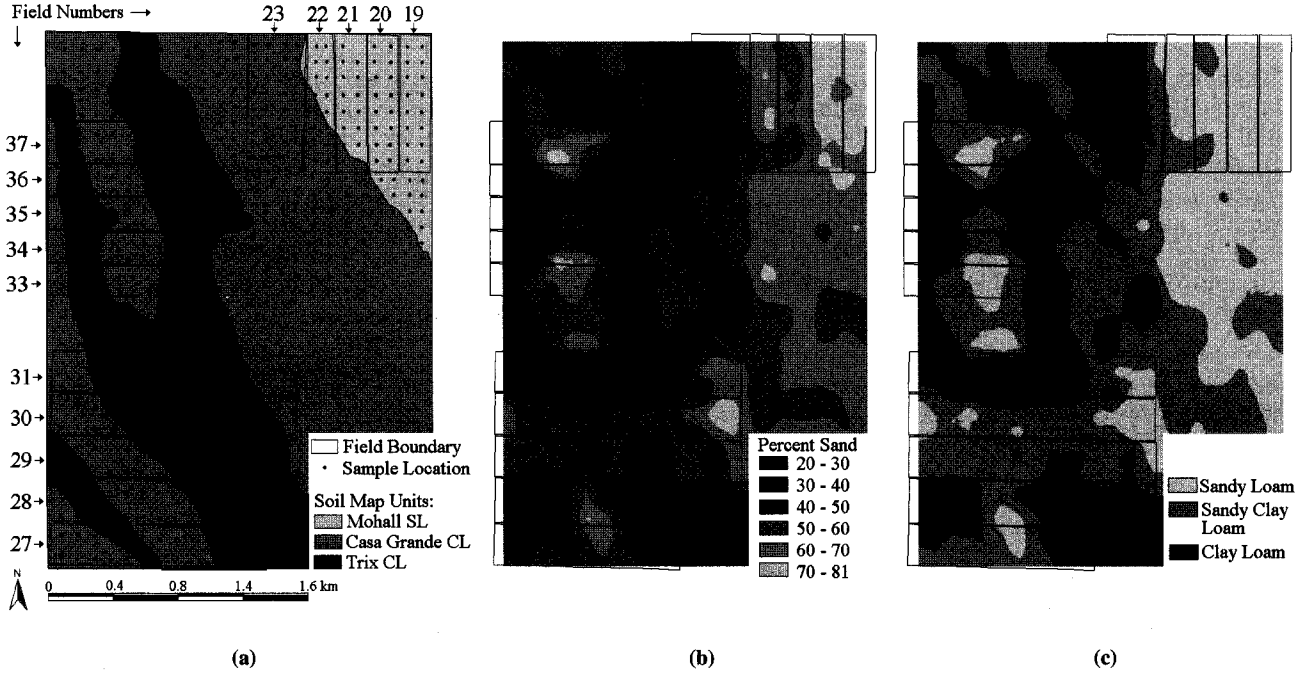

Figure 1–(a) Soil sampling locations, field numbers and NRCS soil mapping units, (b) percent sand map estimated from kriging, and (c) soil textural map determined from the percent sand, silt, and clay kriged maps. Field borders and numbers are shown only for the fields used to evaluate the image-based classification procedures.

were located using surveying techniques as described by Regan et al. (1989). Semivariograms were generated for each textural fraction for all of the 555 sampling locations to separation distances of 2000 m. Five different models (spherical, circular, exponential, Gaussian, and linear) were evaluated to determine which best represented the data using the grid module of Arc/Info version 7.1 (ESRI, 1997) by examining the resulting semivariograms. McBratney and Webster (1986) provide a discussion of the models and parameter estimation techniques. Once the appropriate model was selected, the kriging function in ArcGrid was used to spatially interpolate the data to a 2 m grid. Individual grids were generated for the sand, silt, and clay percentages. Each grid cell was then assigned a USDA textural class of sandy loam, sandy clay loam or clay loam based on the sand, silt, and clay percentages interpolated for that cell.

Multispectral Data Sources and Image Correction

Airborne, SPOT High Resolution Visible (HRV), and Landsat Thematic Mapper (TM) were considered in this study. Characteristics of these three sensor systems and acquisition dates are summarized in table 2. The satellite images selected were acquired the last year soil data were collected (1987) and at the time summer seedbed preparation was completed. However, 1994 was the only year an extensive set of airborne imagery was available for the site. There were no major land leveling operations or changes in field geometry during the 10 years between the beginning of the soil sample collection and the acquisition of the airborne imagery; therefore, it is expected that the soil samples accurately portray the variations in soil texture at the time the airborne imagery was collected. The images were geometrically registered to the GIS coverage containing the soil sampling locations (UTM projection, NAD 27 datum). Ground control points were selected until the root-mean-square error of the first order registration model was less than 1 m. Both satellite images easily encompassed the entire study area in a single image frame. The airborne image was composed from portions of 56 individual video frames, forming a single mosaic of the study area.

Flights of the entire farm occurred on 15 separate dates from April to September. Three different image dates (table 2) were used to build a single mosaic image of the farm that contained only bare soil. The visible and NIR bands were calibrated to units of reflectance utilizing canvas tarps of known reflectance. Ground-based radiometer measurements of a bare field, concurrent with overflights, were also used in the calibration procedure (see Moran, Clarke et al., 1997a, for details of the calibration procedure for airborne data). The data set included imagery from a thermal scanner that was initially considered in the evaluation. In an attempt to normalize the thermal data for differences in air temperature between flight dates, the air temperature was subtracted from the surface temperature. Details on the airborne data set are given by Moran et al. (1996).

The first soil mosaic from the airborne data showed the reflectance of a soil in the same field was different on different dates. These differences were probably a combination of actual changes in the soil surface conditions between flights (tillage or rain compaction of the soil surface, soil moisture, etc.), orientation of the aircraft (pitch or yaw creating different view angles), differences in solar zenith angle at the time of acquisition, and possible errors in the calibration procedures. There were also noticeable differences between coincident image frames taken on the same date that may have been due to the pitch or yaw of the aircraft. To minimize these differences, one image date was taken as the standard, and then multiplication factors were applied to each band of the other frames. These factors ($Factor_{i,b}$) were determined by the following equation:

$$Factor_{i,b} = \frac{R_{i,b}}{R_{stand,b}} \quad (1)$$

where $R_{i,b}$ is the reflectance on day i in band b, and $R_{stand,b}$ is the reflectance from the image date selected as the standard. Reflectance values for the numerator of equation 1 were selected in the image frame adjacent to a frame serving as the standard. As the satellite data sets were single acquisitions, no radiometric calibration was performed.

Statistical and Classification Procedures

The classification process was conducted across two different spatial scales: classification using data for the all of the fields identified by number in figure 1a (farm-level), and classification on a field-by-field basis (field-level). The airborne imagery was used to first identify classification and filtering procedures that provided the best accuracy. Once identified, the same procedures were applied to the SPOT and Landsat images. From all images, single pixels corresponding to the soil sample locations were extracted and imported to a spreadsheet so the correlation between the individual spectral bands and soil textural percentages could be evaluated. Correlation coefficients were calculated for the entire data set and on a field-by-field basis.

Table 2. Sensor characteristics

Sensor*	Spatial Resolution	Acquisition Date		Spectral Bands (μm)	Spectral Region†	Frame Size (km)
Airborne	2 m	12 April 1994‡	1:	0.545-0.555	Green	~ 1 × 1
		02 May 1994	2:	0.645-0.655	Red	
		07 July 1994	3:	0.840-0.860	NIR	
			4:	8.0-12.0	Thermal	
SPOT HRV	20 m	09 April 1989	1:	0.500-0.590	Green	60 × 60
			2:	0.610-0.680	Red	
			3:	0.790-0.890	NIR	
Landsat TM	30 m§	13 April 1989	1:	0.450-0.520	Blue	185 × 185
			2:	0.520-0.600	Green	
			3:	0.630-0.690	Red	
			4:	0.760-0.900	NIR	
			5:	1.55-1.75	SWIR	
			6:	10.4-12.5	Thermal	
			7:	2.08-2.35	SWIR	

* The airborne system was composed of three optical video cameras and a thermal scanner provided by staff at the Dept. of Biological and Irrigation Engineering at Utah State University. HRV is high-resolution-visible, and TM is "Thematic Mapper".

† NIR is near infrared and SWIR refers to shortwave infrared.

‡ For the airborne data the first flight date was used to represent fields 19 to 23, fields 31, 33 to 37 on the second date; fields 27-30 for the third date.

§ Thermal (band 6) is at 120 m spatial resolution.

Unsupervised classification was conducted using the Iterative Self-Organizing Data Analysis Techniques (ISODATA) (Tou and Gonzalez, 1974) using the Imagine 8.3 image processing package (ERDAS, 1997). All bands for each sensor system were used with the exception of the thermal bands in the airborne and Landsat data due to results obtained during the correlation analysis. ISODATA uses iteration to define "clusters" of data in multi-dimensional spectral space. A maximum-likelihood decision rule was used to determine the division of the classes. In some areas, there were isolated groups of pixels that classified differently from those in the surrounding area. These differences may have been induced by small patches of residue or in some cases represented areas that were on the edge of a spectral class. To remove these inclusions, first a convolution filter was applied that used a majority rule with a 7 × 7 window. Next, an 8-pixel clumping algorithm was executed where pixels with the same class were "connected". Based on the results of the clumping algorithm, areas spatially connected with less than 240 pixels were eliminated. For the farm-level classification, the resulting classes were then assigned to a soil class of sandy loam (SL), sandy clay loam (SCL), or clay loam (CL) based on the spectral classes present in fields 27 and 33 as these fields contained a wide range of soil conditions. These sites, plus three others, were also used in the farm level evaluation to derive soil texture maps using supervised classification methods. Spectral patterns corresponding to the soil textural classes were defined at the five "training" sites and then the rest of the image was classified to soil texture based how close the spectral pattern at a particular location matches the one predefined. Supervised classification was attempted in this study, as the soil data were available at the time of analysis. In some cases, supervised classification may be appropriate if soil samples for an area of a farm are already available. However, unsupervised classification can be used to identify areas of a field that have similar spectral properties. Soil samples can then be obtained for the spectral class to identify the soil properties associated with that class. Thus, this farm-level classification was the only occasion supervised classification was attempted, and unless otherwise specified, "classification" refers to the unsupervised classification procedures. For the field-level classification, soil data within each field were used to assign a spectral class to a soil textural class. A total of 60 soil samples, typically a minimum of three per field, were needed in order to assign soil classes for the field level classification.

In addition to applying the above procedures to generate soil maps, the same unsupervised classification methods were applied to fields 33 through 37 with a cotton crop present using the airborne data acquired on 21 July 1994. Unsupervised classification of the image was followed by application of the algorithms to eliminate small, spatially discontinuous classes. The classes were designated "high", "medium", and "low" vegetation using ground-based visual estimation of the percent crop cover in subsections of the field. The resulting vegetation classes were then compared to the soil classes previously defined for these fields.

The accuracy of each classification was assessed by the following formula:

$$PC = \frac{TCC}{TOC} \times 100\% \quad (2)$$

where PC represents the percentage of soil sample points correctly classified as sandy loam, sandy clay loam, or clay loam, and TCC is the total number of points correctly classified and TOC is the total number of observed points.

Evaluation of Differences in Soil Surface Condition on Reflectance

Hand-held radiometer (CropScan MSR) measurements were taken over an area with the same soil type containing different surface conditions. Measurements were all taken within a 15 min period and the locations were within a 15-m-diameter area. The soil surface conditions considered were:

1. Dry smooth soil surface.
2. Wet, smooth soil surface (2 cm of water applied 30 min prior to measurement).
3. Dry soil, smooth, but 5 cm high ridges (10/m) present.
4. Dry soil, cultivated, unplanted bed (approximately 20 cm from bed top to furrow).
5. Wet, cultivated, unplanted bed (2 cm of water applied 30 min prior to measurement).
6. Partially wet, cultivated, unplanted bed (1 cm of water applied 1 h prior to measurement).
7. Dry soil bed, with 5% of the surface covered by crop residue.
8. Dry, flat surface with soil clods up to 8 cm in diameter.

The radiometer consisted of eight silicon detectors filtered to different reflective bands, and was held 1.5 m above the soil surface (0.75-m-diameter area of influence). An infrared thermometer was also side-mounted on the radiometer. Five of the reflective bands were relatively narrow (± ~0.20 μm of central wavelength): blue (0.460 μm), green (0.559 μm), red (0.661 μm), red-edge (0.710 μm), and NIR (0.810 μm). The remaining three bands were similar to bands 3, 4, and 5 of the Landsat TM sensor (table 2) with central wavelengths of 0.660 μm, 0.830 μm, and 1.65 μm, respectively.

Results and Discussion

Kriging Results

Table 3 shows the semivariogram model parameters for sand, silt, and clay textural percentages, and the RSME between the observed and predicted semivariance from the models evaluated. Figure 2 is sample semivariograms for the observed and predicted clay textural data. The exponential model consistently provided the lowest RSME for each of the textural classes. Visual assessment of the semivariograms also indicated that the exponential model provided the best estimate of semivariance across the entire range of separation distances. The circular model predicted a much higher range than the other models, resulting in a continuing increase in predicted semivariance across the separation distances considered (table 3 and fig. 2b). The Gaussian model tended to underestimated semivariance at separation distances greater than 1200 m. There were not large differences in predicted semivariance between the

Table 3. Parameters for the semivariance models determined for the sand, silt, and clay textural percentages

Parameter	Model*				
	Spherical	Circular	Exponential	Gaussian	Linear
	Sand (%)				
c_0	31.2	43.0	10.4	49.9	39.8
c	200.0	219.0	245.6	170.9	190.3
a or r	1679.6	2002.0	774.3	699.5	1308.7
RSME†	29.4	29.9	28.1	33.6	30.9
	Silt (%)				
c_0	10.9	15.7	4.7	11.2	12.3
c	41.3	44.6	50.5	37.3	39.1
a or r	1420.4	2002.0	575.0	533.7	1049.5
RSME	7.2	7.5	6.9	8.2	7.4
	Clay (%)				
c_0	6.4	10.1	0.0	11.7	8.7
c	63.6	70.6	77.3	54.4	60.4
a or r	1611.8	2002.0	735.1	644.1	1225.4
RSME	9.6	9.8	8.9	11.0	10.2

* The models considered for semivariance (γ) were:

Spherical:

$\gamma(h) = c_0 + c;\ h > a$

$\gamma(0) = 0$

$$\gamma(h) = c_0 + c\left[\frac{3h}{2a} - 0.5\left(\frac{h}{a}\right)^3\right];\ 0 < h \le a$$

Circular:

$\gamma(h) = c_0 + c;\ h > a$

$\gamma(0) = 0$

$$\gamma(h) = c_0 + c\left[1 - \frac{2}{\pi}\cos^{-1}\left(\frac{h}{a}\right) + \sqrt{1 - \frac{h^2}{a^2}}\right];\ 0 < h \le a$$

Exponential:

$\gamma(0) = 0$

$$\gamma(h) = c_0 + c\left[1 - \exp\left(\frac{-h}{r}\right)\right];\ h > 0$$

Gaussian:

$\gamma(0) = 0$

$$\gamma(h) = c_0 + c\left[1 - \exp\left(\frac{h^2}{r^2}\right)\right];\ h > 0$$

Linear (with sill):

$\gamma(h) = c_0 + c;\ h > a$

$\gamma(0) = 0$

$$\gamma(h) = c_0 + c\left(\frac{h}{a}\right);\ 0 < h \le a$$

where c_0 is the nugget, a is the range, r non-linear parameter (interpreted as approximately a/3), and h is separation distance in m.

† RMSE is root-mean-square error between observed and predicted semivariance.

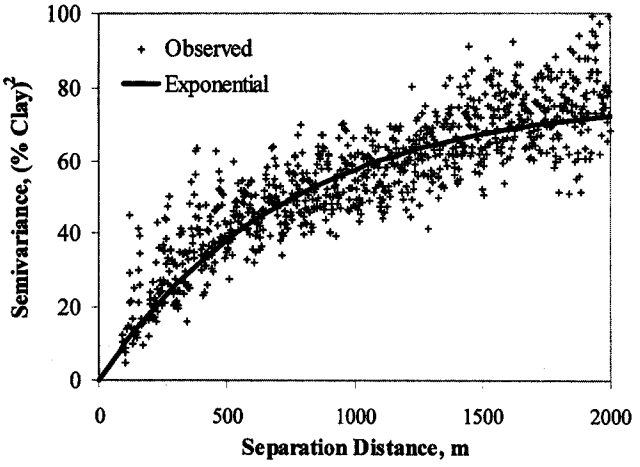

(a) Observed percent clay semivariogram and predicted from the exponental model

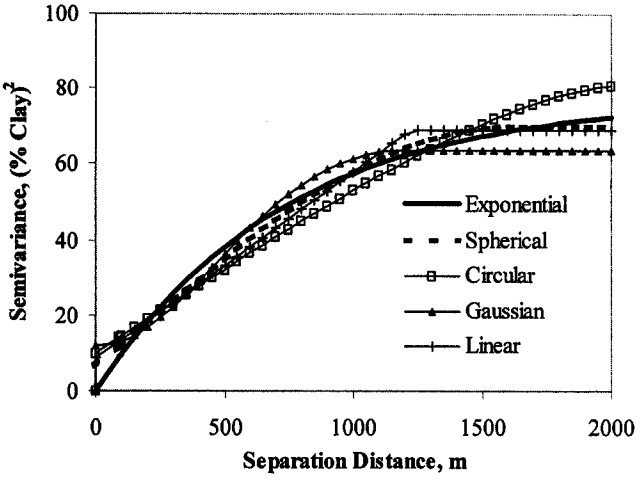

(b) Percent clay semivariograms from the exponential, spherical, circular, Gaussian, and linear models

Figure 2–Percent Clay Semivariograms from (a) observed data and exponential model, and (b) exponential, spherical, circular, Gaussian, and linear models.

linear, spherical and exponential models. The exponential model was used in the remainder of the kriging procedures as it provided slightly better results than the other models considered for all of the textural classes.

The kriged percent sand map using the exponential model for semivariance is shown in figure 1b. Lighter shades of gray correspond to a higher fraction of sand in the soil surface layer. The reduction of the sand, silt and clay kriged maps to a soil textural class map is represented in figure 1c. The map in figure 1c is compared to image derived maps in a following section of this article. The predicted textural content at the points used in the kriging were within 1 textural percent for all the textural classes. There are distinct areas with high sand content apparent in different areas of the farm (fig. 1b). These areas primarily relate to drainage patterns in the area before it was reclaimed for agricultural production. These areas are not always represented in the NRCS soil-mapping units, as the mapping units are not intended to indicate soil variability at fine spatial resolutions. Additionally, Post et al. (1988) found that the Casa Grande series had a surface composed primarily of sandy clay loam at this site, while the NRCS assigns the mapping unit a texture of clay loam.

Correlation Analysis

Correlation coefficients (r) between spectral bands of each sensor and sand, silt and clay percentages are shown in table 4, using data for the entire study area. With the exception of the thermal bands, all coefficients are significantly different than zero (p = 0.05). Also note that r values tend to increase in magnitude with increasing wavelength (excluding thermal data) for all sensor systems. This implies that for the conditions in this study area, Landsat data could have an advantage in distinguishing soil classes due to its increase in spectral range over the airborne and SPOT sensors.

While statistically significant, the correlation coefficients indicate that typically less than 30% of the variation in any given band can be attributed to differences

Table 4. Correlation coefficients between the percent sand, silt or clay and a specific spectral region of a given sensor system over the entire area considered in the analysis

	Spectral Region						
	Blue	Green	Red	NIR	SWIR1	Thermal	SWIR2
	Landsat TM Spectral Band						
	1	2	3	4	5	6	7
$r_{\%Sand,Band}$	0.296*	0.380*	0.462*	0.493*	0.526*	–0.053	0.572*
$r_{\%Silt,Band}$	–0.268*	–0.346*	–0.426*	–0.466*	–0.502*	0.001	–0.547*
$r_{\%Clay,Band}$	–0.309*	–0.394*	–0.473*	–0.494*	–0.524*	0.094	–0.568*
	SPOT Spectral Band						
	1	2	3				
$r_{\%Sand,Band}$	0.400*	0.470*	0.497*				
$r_{\%Silt,Band}$	–0.328*	–0.397*	–0.428*				
$r_{\%Clay,Band}$	–0.450*	–0.518*	–0.539*				
	Airborne Sensor Spectral Band						
	1	2	3	4			
$r_{\%Sand,Band}$	0.359*	0.414*	0.461*	–0.064			
$r_{\%Silt,Band}$	–0.340*	–0.403*	–0.450*	0.091			
$r_{\%Clay,Band}$	–0.359*	–0.403*	–0.449*	0.034			

* Significantly different than 0 (p = 0.05).

in soil texture. Explanation for the remaining variation can be partially found by viewing the gray scale images in the NIR portion of the spectrum from the airborne, SPOT, and Landsat sensors, in figure 3. For example, in figure 3a, there are several differences in reflectance levels that are not related to soil texture. The two dark rectangles in field 35 are due to irrigation in progress. There is also a distinct "corner" in the upper center portion of the field that is an artifact of mosaicing individual frames used to create the image (also visible in field 20). Similar confounding factors can be found in the SPOT and Landsat scenes. The fact that fields 33 and 34 in both figures 3b and 3c appear brighter than the fields above can be attributed to a longer fallow period. The increased fallow period allows for more rain compaction and smoothing of the surface, giving it a brighter appearance when compared to a recently tilled field. Other interfering factors include row direction (north to south versus east to west) and seedbed preparation (flat versus beds).

Figure 4 presents correlation coefficients between spectral bands of each sensor on a field-by-field basis with percent sand. Values outside the horizontal bars are significantly different than zero (p = 0.05). In some cases, low correlation values can be attributed to the fact there was very little variation in soil texture in a particular field. This is most likely the case when considering fields 19, 20 and 22, as all of these fields have consistently high sand percentages (fig. 1b). For the Landsat and SPOT scenes, field 30 was undergoing a tillage operation (fig. 3b,c), and thus low correlation values in this field were obtained for those sensors. For the airborne data, field 29 had varying levels of residue and various tillage conditions; so again, there was poor correlation between the spectral data and soil texture. Despite these limitations, from both the farm level (table 4) and field-by-field correlation analysis (fig. 4), there is generally a statistically significant relationship between the spectral data and soil texture. For the most part, percent sand is positively correlated with reflectance, while silt and clay generally show a negative correlation. This is confirmed by viewing the NIR images in figure 3, as areas with high sand (fig. 1b) tend to have a brighter appearance. The soils at this site with higher sand content tend to have lower organic matter content (table 1), which may be responsible for the higher reflectance values over the sandier areas. It is important to note that these results are specific to this site, as many factors can contribute to soil spectral properties.

The thermal data were not highly correlated with any of the soil textures with exception of field 31 in the airborne data (fig. 4). This correlation is likely spurious, as the east side of the field, where there is a definite increase in sand content, was recently tilled at the time the image was taken. Disturbing the soil surface exposed moisture and cooler soil, thus the negative correlation between sand content and the thermal data. Further regression analysis was not attempted, as Suliman and Post (1988), using the soil samples from this data set, were only able to obtain coefficient of determination values (r^2) ranging from 0.4 to 0.5 between various combinations of TM spectral bands. Their tests were carried out in a laboratory setting under carefully controlled conditions.

Classification Results

Based on the results from the previous section, a robust, empirical relationship could not be established between the image data and fractional content of sand, silt, or clay for

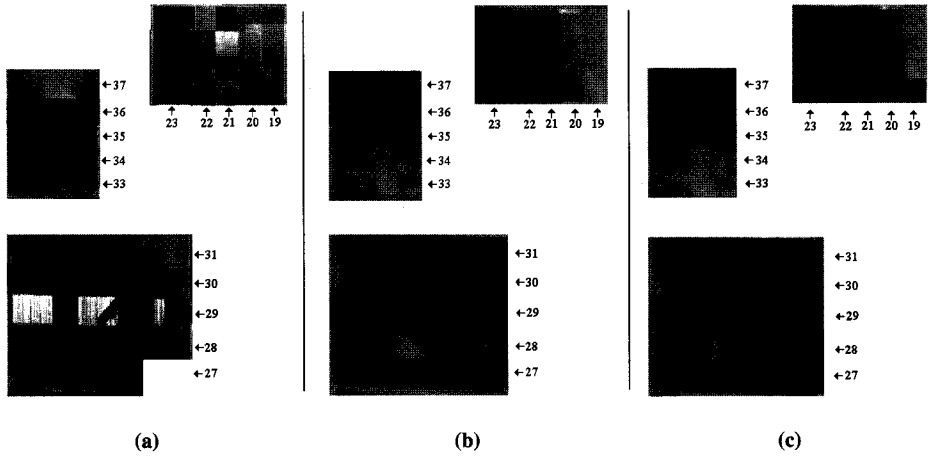

Figure 3–Near infrared images of the study area from (a) airborne sensor, (b) HRV sensor on SPOT, and (c) TM sensor on Landsat. Numbers are shown to identify individual fields referred to in the next.

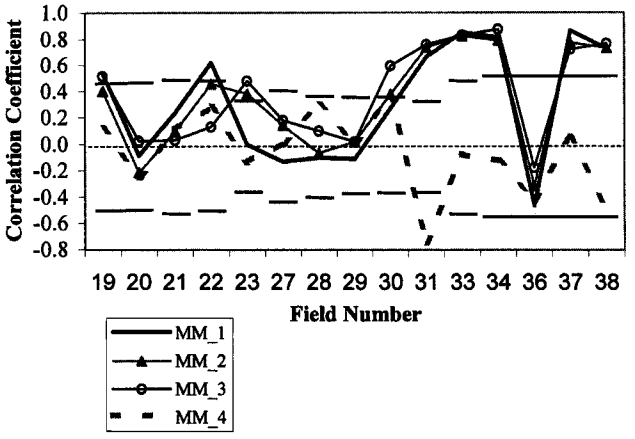

(a) Airborne sensor data

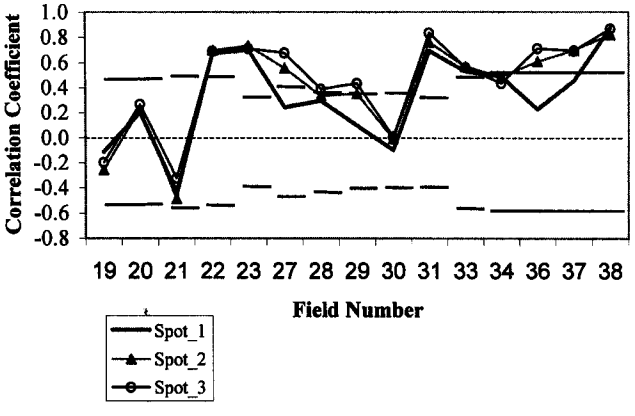

(b) SPOT

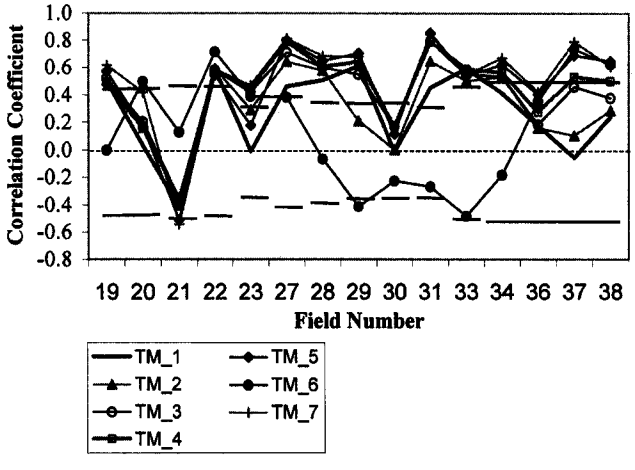

(c) Landsat

Figure 4–Correlation between sensor data and percent sand on a field-by-field basis. Points outside of the horizontal bars are significantly different than 0 (p = 0.05).

this site. Therefore, the next step was to evaluate the ability to relate the images to soil textural class using spectral classification techniques. Table 5 shows the overall accuracy assessment for classification conducted at the farm level. Correct classification of the soil textural classes of 50% or less for all of the sensor systems is very poor.

Table 5. Accuracy assessment for the spectral classification procedures executed across the entire study area

Classification Technique	Sensor System		
	Airborne	SPOT	Landsat
	Soil Types Correctly Classified (%)		
Supervised	47	NA	NA
Unsupervised	51	51	48

The same factors previously discussed that impacted the correlation coefficients are probably responsible for poor accuracy at the farm level. The use of supervised versus unsupervised showed no clear advantage when considered at the farm level. Supervised classification was not considered at the field level, as there was often insufficient data with which to construct training sites at that scale.

There was tremendous improvement in the accuracy achieved when unsupervised classification was conducted on a field-by-field level (table 6) compared to the farm level results (table 5). Much of this accuracy increase results from the relatively uniform surface in a single field when compared to variations in soil surface conditions across the entire farm. The slightly higher accuracy achieved with the Landsat data could be attributed to its increased spectral range.

The resulting soil maps from field-by-field classification procedures of the airborne, SPOT, and Landsat data are shown in figure 5. In order to compare differences in spatial patterns, the three-class map generated from kriged data (fig. 1c) was subtracted from the spectrally derived maps. The results of the subtraction are shown in figure 6, where shaded areas indicate disagreement. Based on this figure, it was determined that the percent area classified differently from the kriged map were 29%, 21%, and 20% for the airborne, SPOT, and Landsat derived maps, respectively. The major spatial groupings of soil type are similar in each of the maps. Most differences occur in the border area between classes. The map derived from the airborne data (fig. 5a) showed there were several areas in field 30 classified as sand that did not appear in the other classifications nor were they indicated by observed data. This field contained barley residue at the time of image

Table 6. Accuracy assessment of the spectral classification procedures executed on a field-by-field basis

Field Number	Sensor System		
	Airborne	SPOT	Landsat
	Soil Types Correctly Classified (%)		
27	73	91	82
28	58	92	92
29	60	80	87
30	52	76	90
31	77	80	90
33	93	93	87
34	75	81	100
35	100	79	93
36	100	100	100
37	86	86	100
19	100	100	100
20	100	100	100
21	67	80	80
22	94	94	94
23	81	94	88
Overall	81	88	92

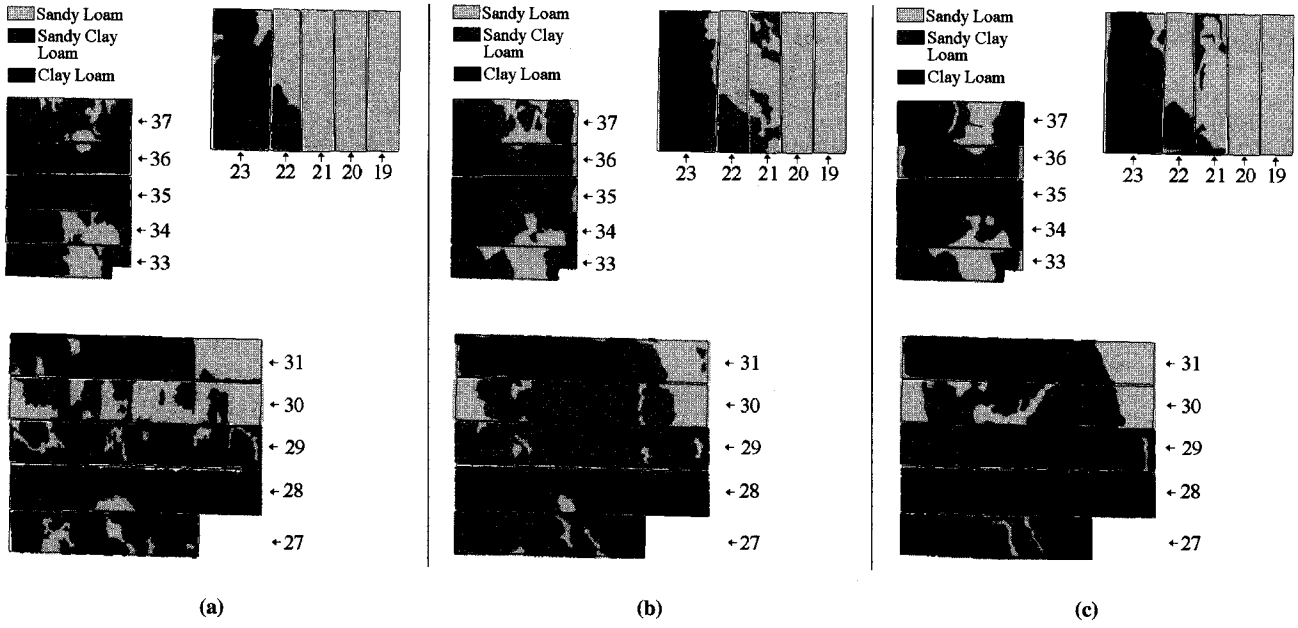

Figure 5–Soil maps derived from the field-level, unsupervised classification of the (a) airborne, (b) SPOT, and (c) Landsat data. Numbers are shown to identify individual fields referred to in the text.

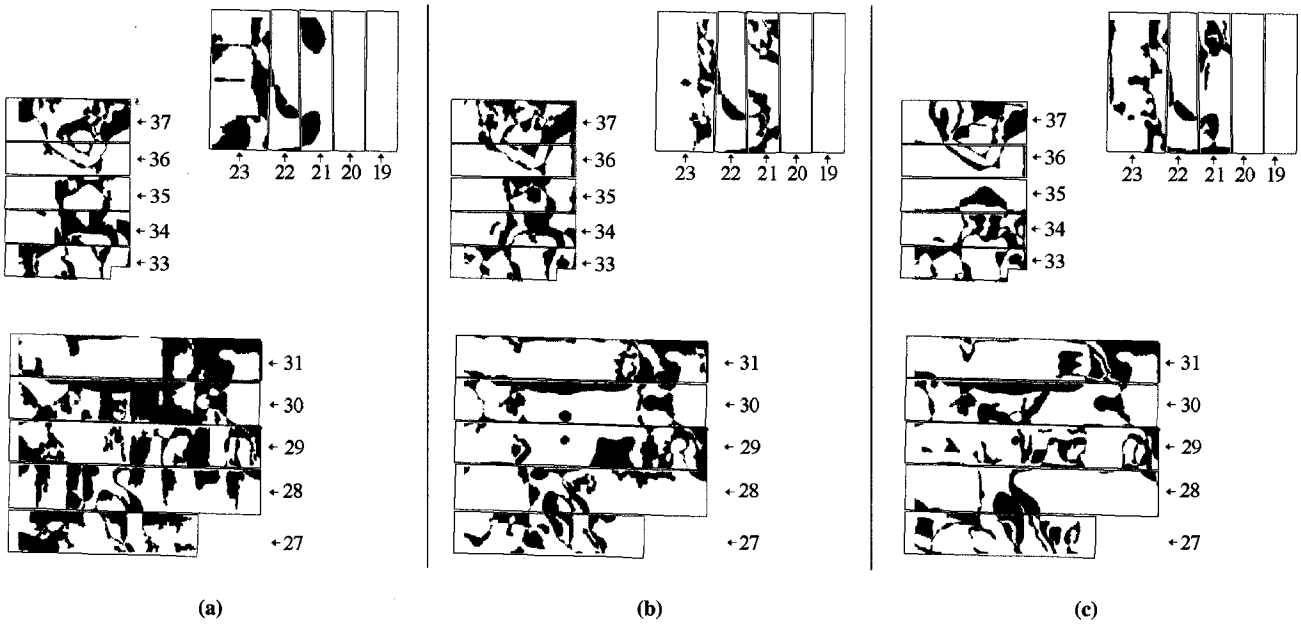

Figure 6–Results of the subtraction of the soil maps derived from the (a) airborne, (b) SPOT, and (c) Landsat data (fig. 5) by the three-class kriged soil map (fig. 1c). Shaded areas represent differences. Numbers are shown to identify individual fields referred to in the text.

acquisition, increasing the apparent brightness of the surface. The soil surfaces with high sand content are also brighter, thus the residue resulted in areas of the field being incorrectly classified as sandy loam.

The middle of field 27 contains a sand lens that runs north to south. Note that the apparent size of the sandy area is largest in figure 5a (airborne derived) and smallest in figure 5b (Landsat derived). Differences in class size are probably related to the spatial resolution of the sensors, with the airborne data having the highest and Landsat the lowest resolution (table 2). This is one of the few cases where the differences in spatial resolution appeared to have any significant impact. A majority of the different soil textural classes considered have dimensions in excess of 200 m, well within the spatial resolution of all of the sensors. If the variations in soil texture are more heterogeneous and limited to smaller, continuous areas than was present at this site, the differences in the spatial resolution of the different sensor systems could impact soil texture mapping accuracy.

Where the soil surface was uniform at the time of image acquisition, it is speculated that patterns derived from the images would be more accurate than those from derived the interpolated data. Additionally, only 60 soil sample locations were used to assign classes in the image-based maps classified on a field-by-field basis, while

303 locations were used for the kriged map. The number of points needed for the image-based method could have been substantially reduced if the soil surface was uniform across the farm.

Vegetation Classes

Before any soil zone can be termed a "management zone", it is important to consider if differences in soil properties have a significant impact on crop development. Figure 7 presents visual observations of the field conditions near the time of image acquisition, a gray-scale NIR image of the field, and the vegetation classes derived from unsupervised classification. Note that the visual observations were obtained by viewing the field from the road and represent what the observer considered the average conditions in that section of the field. The vegetation classification of fields 33 to 37 shown in figure 7 can be useful to determine if the soil zones previously defined appear to impact crop development. For example, in fields 33 and 34, the vegetation class patterns roughly match the soil classes previously derived from the bare soil images (fig. 5). In these fields, areas classified as low canopy density tend to correspond to areas of higher sand content. The reduced water holding capacity of sandy areas and the fact that these fields are given uniform irrigation applications may help explain the general agreement in the distribution of these classes.

The agreement between the vegetation and soil classes is not as clear in fields 35 to 37. In field 37, portions of the field had been divided into plots by removing plants between treatments. This altered the apparent plant density independent of soil type. In fields 35 and 36, different cotton varieties were grown within the field. The division in the vegetation classes often corresponds to the division between different varieties. Thus, this is a good indication that soil differences were not responsible for these patterns. Another interfering factor can be the condition of the soil background. For example, the far-left block of field 35 in figure 7 was primarily classified as "high" vegetation, while the adjacent block to the right was classified as "low" vegetation. However, field observations indicated that both areas had the same crop cover, but the far-left block had a lower crop height (fig. 7). The left-most block also had a dry soil surface, while the soil in the block to the right was still moist from a recent irrigation. Near infrared radiation is more strongly absorbed by water than visible, and part of the spectral response that defines a relative increase in vegetation is an increase in NIR reflectance. Thus the wet versus dry soil background can falsely indicate a decrease in vegetation.

The previous discussion lends support to the idea that more accurate vegetation classes could be derived after canopy closure. However, unsupervised classification of images for the same fields later in the season generally resulted in a significant reduction in soil classes, including some believed to be related to soil type. Under complete crop cover, the sensitivity to canopy density is decreased in the visible and NIR part of the spectrum. Crop cover greater than 50% is desirable, so that soil background conditions in addition to soil moisture do not begin to dominate the spectral response.

In summary, if soil variation does impact the crop's development, the number of vegetation class patterns is expected to be equal to or greater than the number of soil classes. There could be more vegetation classes than soil classes because factors such as management practices, insect damage, irrigation uniformity, and weed pressure impact a crop's growth in addition to soil type. However, if some soil classes that do not occur in vegetation classes, the soil class may not need to become a management unit.

Crop Cover:	90%	100%		95%		95%	
Height (cm):	90	110		110		120	
Soil:	Wet	Wet		Wet		Wet	
Variety:	NA	NA		NA		NA	
Crop Cover:	80%	90%	90%	90%	90%	90%	80%
Height (cm):	90	100	100	90	90	90	80
Soil:	Dry	Dry	Dry	Dry	Dry	Dry	Dry
Variety:	NA	U90	NA	NA	U90	U90	U54
Crop Cover:	85%	85%	90%	90%	90%	95%	95%
Height (cm):	75	90	110	110	110	110	110
Soil:	Dry	Wet	Wet	Wet	Wet	Wet	Wet
Variety:	NA	U90	U54	U90	U54	U90	U90
Crop Cover:	100%	100%		90%		90%	
Height (cm):	100	100		90		90	
Soil:	Wet	Wet		Wet		Wet	
Variety:	Pima	Pima		Pima		Pima	
Crop Cover:	100%	100%		90%		90%	
Height (cm):	90	90		70		90	
Soil:	Wet	Wet		Dry		Dry	
Variety:	Pima	Pima		Pima		Pima	

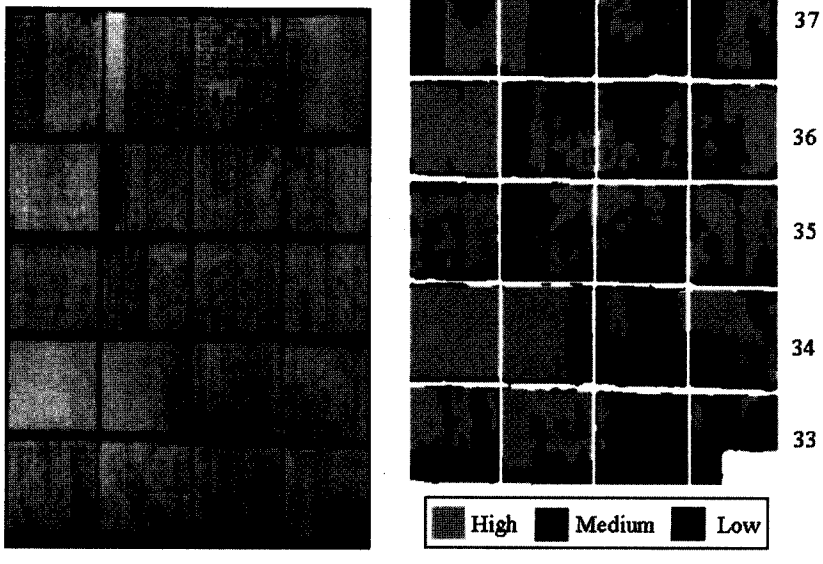

(a) (b) (c)

Figure 7–Field observations (a), NIR image (b), and vegetation classes (c) for fields 33 to 37. Field observations are based on a visual assessment of percent crop cover, crop height, and surface soil moisture near the time of image acquisition. Different varieties of cotton were grown in these fields: NA indicates information on the specific variety was not available; U90 is Upland (*Gossypium hirsutum*) Delta Pine 90; U54 is an Upland Delta Pine 5415 variety; and Pima (*G. barbadense*).

If nutrients and water are over-applied to the area; however, it is possible that the soil type influences could be masked.

Impact of Soil Surface Conditions on Multispectral Data

As differences in soil tillage, moisture, and residue conditions were found to impact the accuracy of the image classification results, the hand-held radiometer data collected were used to quantify the impact of these differences on surface reflectance. Figure 8 shows the reflectance measured with the hand-held radiometer for various soil surface conditions. For this site, a wet soil surface resulted in a significant decrease in the soil's reflectance across all of the bands considered. The presence of a small amount of crop residue did not have a large impact on the visible bands; however, it did result in a 5% difference in the NIR bands (0.810 and 0.830 μm). The smoother soil surfaces had higher reflectance values than the bed and surface with soil clods as both the beds and clods cast shadows over a portion of the surface. The impact that soil surface conditions can have on the ability of reflectance data to accurately map soil texture can be illustrated by comparing tables 7 and 8. Table 7 contains the range in the reflectance values presented in figure 8. Table 8 presents the average reflectance determined from the airborne data over areas of known soil texture. The

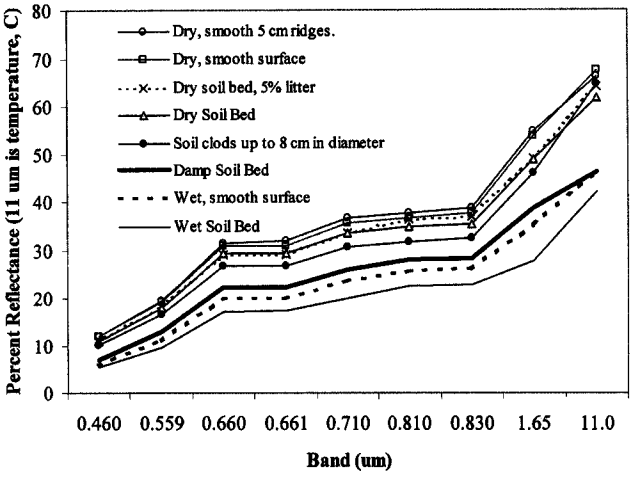

Figure 8–Percent reflectance (or surface temperature for the thermal band) measured with a hand-held radiometer for different soil surface conditions. All measurements were taken within a 15-m-diameter area.

Table 7. Summary statistics for the hand-held radiometer data presented in figure 8

	Center Wavelength (μm)							
Statistic	0.460	0.559	0.660	0.661	0.710	0.810	0.830	1.650
	Statistics Based on All of the Soil Surface Conditions (range and average have units of percent reflectance)							
Range	6.6	9.9	14.4	14.6	16.4	15.2	15.8	27.1
Average	9.3	15.7	25.8	26.0	29.9	31.7	32.3	44.3
Range/Average (%)	70	63	56	56	55	48	49	61
	Statistics Based on Dry Soil Surfaces Only (range and average have units of percent reflectance)							
Range	1.9	3.0	4.9	5.1	5.9	6.1	6.2	9.0
Average	11.2	18.3	29.4	29.6	33.9	35.4	36.2	50.5
Range/Average (%)	17	17	17	17	17	17	17	18

Table 8. Reflectance values from the calibrated airborne sensor data over different soil types

	Center Wavelength (μm)		
Surface	0.550	0.650	0.850
	Reflectance (%)		
Field 33			
Sandy loam	21.1	28	36.8
Clay loam	16.9	20.7	28.7
Difference	4.2	7.3	8.1
Field 28			
Sandy loam	16.3	23.4	33.3
Clay loam	12.6	18.4	25.3
Difference	3.7	5	8

difference in reflectance between dry and wet soil shown in table 7 is much greater than the difference in reflectance of soils with very different textures. Even when reflectance differences due to surface moisture are eliminated, reflectance differences caused by tillage differences have the same level of influence on reflectance as those caused by soil type differences. For example, the range in reflectance for a wet versus dry surface at 0.660 μm is 14%, and 4.9% due to changes in surface roughness under dry conditions (table 7). At approximately the same wavelength (0.650 μm), the difference in reflectance of a sandy loam and clay loam soil is between 5 and 7% reflectance.

Summary and Conclusions

Many factors that can impact a soil's apparent reflectance are not related to the soil's physical properties such as tillage practices, crop residue, row orientation and surface moisture. Therefore, the use of multispectral imagery is best suited for farms with fields that have uniform tillage and moisture conditions at the time of image acquisition. The soil property of interest should exhibit a spectral response. For example, in this study soil with higher sand content tended to have a higher reflectance in the visible and NIR portion of the spectrum. If such conditions are present, unsupervised classification provides the ability to identify potential soil zones before soil samples are taken. The number of soil samples needed to map soil properties with remotely sensed data could then be significantly reduced when compared to spatial interpolation techniques. Utilization of quantitative techniques to classify soil management zones with data from low flying aircraft is more challenging than using data from satellites due to the small area that can be contained in a single frame. Often differences between image frames result in the need to classify parts of the farm on a frame-by-frame basis. While this can result in a useful soil map, it is a labor-intensive process and may increase the number of soil samples needed for accurate classification. The use of multi-temporal imagery will probably require individual classification due to changes in soil surface conditions between images. One advantage offered by remotely sensed data is the ability to compare soil maps to crop density patterns. Such a tool can be a significant aid in determining if differences in soil texture warrant modified management practices. However, as with spectral soil classes, interpretation of the vegetation classes should take into account factors other than soil type that

can impact crop development (e.g., crop type and variety, pest damage, and soil surface moisture).

ACKNOWLEDGMENTS. The authors are very grateful to Dr. Don Post in the department of Soil, Water and Environmental Science at the University of Arizona for providing us with the soil data used in this study. Additionally, this study would not have been possible without the imagery provided by Susan Moran, Tom Clarke and Paul Pinter of the USDA, ARS, U.S. Water Conservation Laboratory, Phoenix, Arizona.

REFERENCES

Bausch, W. C., H. R. Duke, and C. J. Iremonger. 1996. Assessment of plant nitrogen in irrigated corn. In *Proc. 3rd Int. Conf. on Precision Agriculture*, eds. P. C. Robert, R. H. Rust, and W. E. Larson, 23-32. Madison, Wis.: ASA.

Bell, J. C., C. A. Butler, and J. A. Thompson. 1995. Soil-terrain modeling for site-specific agricultural management. In *Site-Specific Management for Agricultural Systems*, eds. P. C. Robert, R. H. Rust, and W. E. Larson, 209-228. Madison, Wis.: ASA.

Blackmer, A. M., and S. E. White. 1996. Remote sensing to identify spatial patterns in optimal rates of nitrogen fertilization. In *Proc. 3rd Int. Conf. on Precision Agriculture*, eds. P. C. Robert, R. H. Rust, and W. E. Larson, 33-42. Madison, Wis.: ASA.

Bushnell, T. M. 1932. A new technique in soil mapping. *American Soil Survey Assoc. Bull.* 13: 74-81.

Cambardella, C. A., T. S. Colvin, D. L. Karlen, S. D. Logsdon, E. C. Berry, J. K. Radke, T. C. Kaspar, T. B. Parkin, and D. B. Jaynes. 1996. Soil property contributions to yield variation patterns. In *Proc. 3rd Int. Conf. on Precision Agriculture*, eds. P. C. Robert, R. H. Rust, and W. E. Larson, 189-196. Madison, Wis.: ASA.

Dalal, R. C., and R. J. Henry. 1986. Simultaneous determination of moisture, organic carbon, and total nitrogen by near infrared reflectance spectrophotometry. *Soil Sci. Am. J.* 50: 120-123.

ERDAS. 1997. *ERDAS Field Guide.* Atlanta, Ga.: ERDAS.

ESRI. 1997. *ArcInfo,* Ver. 7.1. Redlands, Calif.: Environmental Systems Research Institute, Inc.

Ferguson, R. B., C. A. Gotway, G. W. Hergert, and T. A. Peterson. 1996. Soil sampling for site-specific nitrogen management. In *Proc. 3rd Int. Conf. on Precision Agriculture*, eds. P. C. Robert, R. H. Rust, and W. E. Larson, 13-22. Madison, Wis.: ASA.

Jaynes, D. B. 1996. Improved soil mapping using electromagnetic induction surveys. In *Proc. 3rd Int. Conf. on Precision Agriculture*, eds. P. C. Robert, R. H. Rust, and W. E. Larson, 169-179. Madison, Wis.: ASA.

McBratney, A. B., and R. Webster. 1986. Choosing functions for semi-variograms of soil properties and fitting them to sampling estimates. *J. Soil Sci.* 37(4): 617-639.

Milfred, C. J., and R. W. Kiefer. 1976. Analysis of soil variability with repetitive aerial photography. *Soil Sci. Soc. Am. J.* 40(4): 553-557.

Moran, S. M., T. R. Clarke, J. Qi, and P. J. Pinter Jr. 1996. MADMAC: A test of multispectral airborne imagery as a farm management tool. In *Proc. 26th Symp. on Remote Sens. Environ.*, 612-617, Vancouver, B.C., 25-29 March. Int. Center for Remote Sensing of Environment, UMBC Technology Center, Baltimore, Md.

Moran, S. M., T. R. Clarke, J. Qi, E. M. Barnes, and P. J. Pinter. 1997a. Practical techniques for conversion of airborne imagery to reflectances. In *Proc. 16th Biennial Workshop on Videography and Color Photography in Resource Assessment*, 82-95. Bethesda, Md.: Am. Soc. Photogram. & Remote Sensing.

Moran, S. M., Y. Inoue, and E. M. Barnes. 1997b. Opportunities and limitations for image-based remote sensing in precision crop management. *Remote Sensing Environ.* 61(3): 319-346.

Nielsen, D. R., O. Wendroth, and M. B. Parlange. 1995. Opportunities for examining on-farm soil variability. In *Site-Specific Management for Agricultural Systems*, eds. P. C. Robert, R. H. Rust, and W. E. Larson, 95-132. Madison, Wis.: ASA.

Pocknee, S., B. C. Boydell, H. M. Green, D. J. Waters, and C. K. Kvien. 1996. Directed soil sampling. In *Proc. 3rd Int. Conf. Precision Agriculture*, eds. P. C. Robert, R. H. Rust, and W. E. Larson, 159-168. Madison, Wis.: ASA.

Post, D. F., C. Mack, P. D. Camp, and A. S. Suliman. 1988. Mapping and characterization of the soils on the University of Arizona Maricopa Agricultural Center. In *Proc. Hydrology and Water Resources in Arizona and the Southwest* 18: 49-60. Tucson, Ariz.: Arizona-Nevada Academy of Science.

Regan, J. J., D. F. Post, and R. S. Rauschkolb. 1989. Mapping the Maricopa Agricultural Center using a geographic information system. *In Proc. Hydrology and Water Resources in Arizona and the Southwest* 19: 47-58. Tucson, Ariz.: Arizona-Nevada Academy of Science.

Salisbury, J. W., and D. M. D'Aria. 1992. Infrared (8-14 μm) remote sensing of soil particle size. *Remote Sensing Environ.* 42(2): 157-165.

Shonk, J. L., L. D. Gaultney, D. G. Schulze, and G. E. Van Scoyoc. 1991. Spectroscopic sensing of organic matter content. *Transactions of the ASAE* 34(5): 1978-1984.

Suliman, A. S., and D. F. Post. 1988. Relationship between soil spectral properties and sand, silt, and clay content of the soils on the University of Arizona Maricopa Agricultural Center. In *Proc. Hydrology and Water Resources in Arizona and the Southwest* 18: 61-65. Tucson, Ariz.: Arizona-Nevada Academy of Science.

Thompson, W. H., and P. C. Robert. 1995. Evaluation of mapping strategies for variable rate applications. In *Site-Specific Management for Agricultural Systems*, eds. P. C. Robert, R. H. Rust, and W. E. Larson, 303-323. Madison, Wis.: ASA.

Tou, J. T., and R. C. Gonzalez. 1974. *Pattern Recognition Principals.* Reading, Mass.: Addison-Wesley.

USDA-SCS. 1991. Soil Survey of Pinal County, Arizona, Western Part. USDA-SCS in cooperation with Arizona Agricultural Experiment Station, Tucson, Ariz.

Verma, K. S., R. K. Saxena, A. K. Barthwal, and S. N. Deshmukh. 1994. Remote sensing technique for mapping salt affected soils. *Int. J. Remote Sensing* 15(9): 1901-1914.

Wiegand, C. L., J. D. Rhoades, D. E. Escobar, and J. H. Everitt. 1994. Photographic and videographic observations for determining and mapping the response of cotton to soil salinity. *Remote Sensing Environ.* 49(3): 212-223.

Yang, C., and G. L. Anderson. 1996. Determining within-field management zones for grain sorghum using aerial videography. In *Proc. 26th Symposium on Remote Sens. Environ.*, 606-611, Vancouver, B.C., 25-29 March. Int. Center for Remote Sensing of Environment, UMBC Technology Center, Baltimore, Md.